Uncovering the psychoactivity of a cannabinoid from liverworts associated with a legal high

Journal Article

Author(s):
Chicca, Andrea; Schafroth, Michael A.; Reynoso-Moreno, Inés; Erni, Reto; Petrucci, Vanessa; Carreira, Erick M. [iD]; Gertsch, Jürg

NEUROPHYSIOLOGY

Uncovering the psychoactivity of a cannabinoid from liverworts associated with a legal high

A. Chicca[1], M. A. Schafroth[2], I. Reynoso-Moreno[1], R. Erni[2], V. Petrucci[1], E. M. Carreira[2]*, J. Gertsch[1]*

Phytochemical studies on the liverwort *Radula* genus have previously identified the bibenzyl (−)-*cis*-perrottetinene (*cis*-PET), which structurally resembles (−)-Δ^9-*trans*-tetrahydrocannabinol (Δ^9-*trans*-THC) from *Cannabis sativa* L. *Radula* preparations are sold as cannabinoid-like legal high on the internet, even though pharmacological data are lacking. Herein, we describe a versatile total synthesis of (−)-*cis*-PET and its (−)-*trans* diastereoisomer and demonstrate that both molecules readily penetrate the brain and induce hypothermia, catalepsy, hypolocomotion, and analgesia in a CB1 receptor–dependent manner in mice. The natural product (−)-*cis*-PET was profiled on major brain receptors, showing a selective cannabinoid pharmacology. This study also uncovers pharmacological differences between Δ^9-THC and PET diastereoisomers. Most notably, (−)-*cis*-PET and (−)-*trans*-PET significantly reduced basal brain prostaglandin levels associated with Δ^9-*trans*-THC side effects in a CB1 receptor–dependent manner, thus mimicking the action of the endocannabinoid 2-arachidonoyl glycerol. Therefore, the natural product (−)-*cis*-PET is a psychoactive cannabinoid from bryophytes, illustrating the existence of convergent evolution of bioactive cannabinoids in the plant kingdom. Our findings may have implications for bioprospecting and drug discovery and provide a molecular rationale for the reported effects upon consumption of certain *Radula* preparations as moderately active legal highs.

INTRODUCTION

Cannabinoids have a wide range of actual and potential therapeutic applications, and marijuana is widely used not only for its recreational but also for its medicinal properties (*1*, *2*). To date, the plant *Cannabis sativa* L. is the only known natural source of CB1 cannabinoid receptor (CB1R) activators, with Δ^9-*trans*-tetrahydrocannabinol (Δ^9-*trans*-THC) being the most potent partial agonist (*3*, *4*). The THC scaffold was presumed unique to the *Cannabis* plant genus until the bibenzyl *cis*-THC, (−)-*cis*-perrottetinene (*cis*-PET) (Fig. 1), was isolated from the liverwort *Radula perrottetii* Gottsche ex Steph in 1994 by Asakawa and co-workers and later from *Radula marginata* Taylor ex Gottsch (*5*, *6*). Further, Cullman and Becker isolated *cis*-PET from *Radula laxiramea* Steph (*7*). Bryophytes are a distinctive group of an early-diverged lineage of nonvascular land plants comprising more than 20,000 species (Fig. 1). This division includes mosses, hornworts, and liverworts (*8*). Liverworts often generate the opposite stereochemical configuration in secondary metabolite biosynthesis compared with higher plants (*9*). This is also the case for the cis configuration in the cyclohexene ring in *cis*-PET compared with Δ^9-*trans*-THC. The absolute stereochemistry of *cis*-PET was fully structurally characterized in 2008 (*10*). Comparatively little attention has been paid to the liverworts for use in human diet or medicine to date (*9*). Worldwide anecdotal reports both affirm and refute the effectiveness of consuming *R. marginata* preparations inducing a legal cannabis-like high. However, the pharmacology of this natural product remains unknown. *R. marginata* is endemic to New Zealand and Tasmania, and collected dried samples are currently sold via the internet as an emerging recreational drug or as

incense (see Acknowledgments). A molecular understanding of the effects of PET is essential to anticipate potential toxicological or recreational effects in humans. On the basis of a previously established stereodivergent synthesis of Δ^9-THCs (*11*–*13*), we report a versatile total synthesis of natural *cis*-PET and its (−)-*trans* diastereoisomer (Figs. 2 and 3). This enabled a comparative study of PET and Δ^9-THC structure-activity relationships for CB1R and CB2R activation, respectively, as well as cannabimimetic and biochemical effects in mice. To further investigate the pharmacological effects of the liverwort cannabinoid, we measured the bioavailability of *cis*-PET to the brain and profiled this natural product on major central nervous system (CNS) receptors. The CB1R-mediated psychoactive pharmacology is characterized by a typical central effect pattern in mice, generally referred to as the "tetrad test," which includes antinociception, hypothermia, catalepsy, and locomotion inhibition (*14*). A full assessment of both PET diastereoisomers on the endocannabinoid system (ECS) was performed. This study not only provides a molecular basis on which to assess the mode of action and emerging recreational use of smoked *Radula* liverwort preparations as legal high but also allows a direct comparison with Δ^9-THC for potential therapeutic applications.

RESULTS

Stereodivergent total synthesis of cis- and trans-PET

We previously introduced stereodivergent catalysis to enable the synthesis of all stereoisomers of a target, applying it to the synthesis of Δ^9-THCs (*11*–*13*). Maintaining this stereodivergent step, the strategy was adapted to synthesize sufficient amounts of PETs for biological testing and relied on a S_NAr cyclization to assemble the dihydrobenzopyran core (*15*). Following a stereodivergent step using iridium- and amine-catalyzed aldehyde allylation (**1** + **2** → **3**), the S_NAr precursors **4** were prepared through ring-closing metathesis, oxidative esterification, and subsequent Grignard addition (Fig. 2).

[1]Institute of Biochemistry and Molecular Medicine, NCCR TransCure, University of Bern, Bühlstrasse 28, 3012 Bern, Switzerland. [2]Department of Chemistry and Applied Biosciences, Laboratory of Organic Chemistry, ETH Zurich, Vladimir-Prelog-Weg 3, 8093 Zürich, Switzerland.
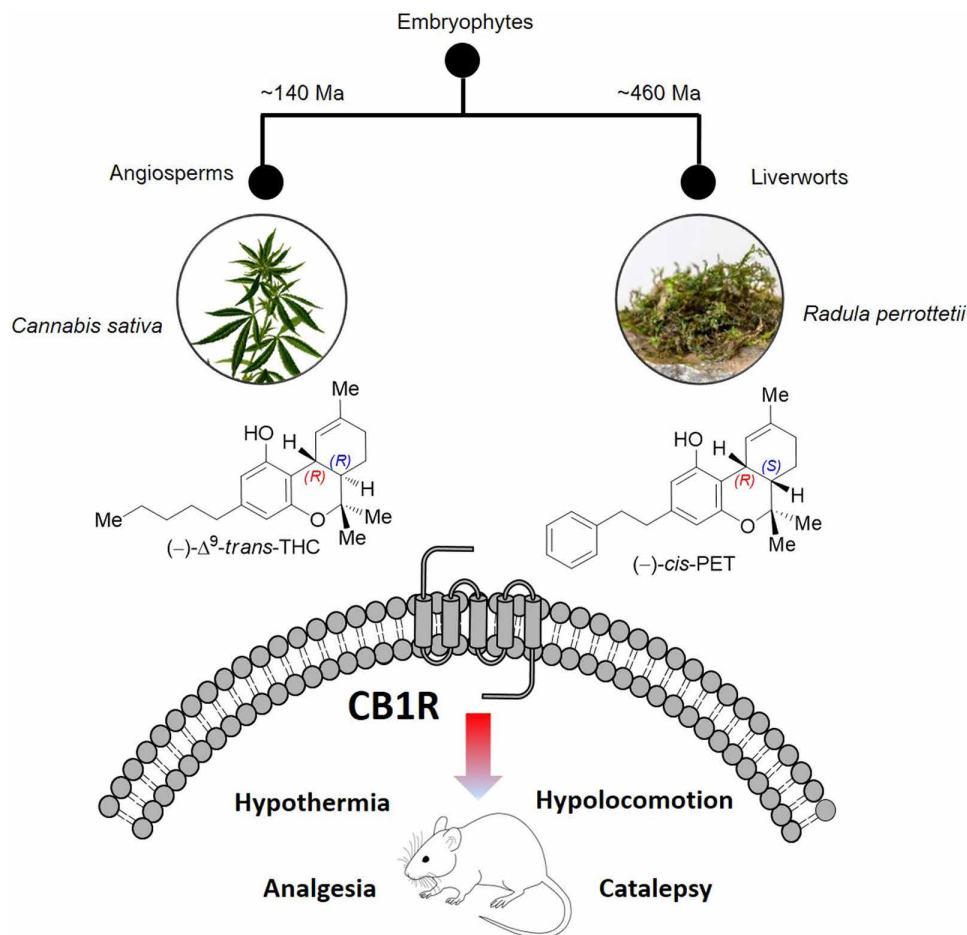*Corresponding author. Email: gertsch@ibmm.unibe.ch (J.G.); carreira@org.chem.ethz.ch (E.M.C.)

Fig. 1. Phylogenetic separation of bryophytes and angiosperms and convergent evolution of the tetrahydrocannabinoid scaffold in (−)-*trans*-THC and (−)-*cis*-PET. Both cannabinoids act as partial agonists on CB1 receptors in vitro and in vivo. Ma, mega-annum. Photo credit: S. Fischer (D-CHAB, LOC, ETH Zurich).
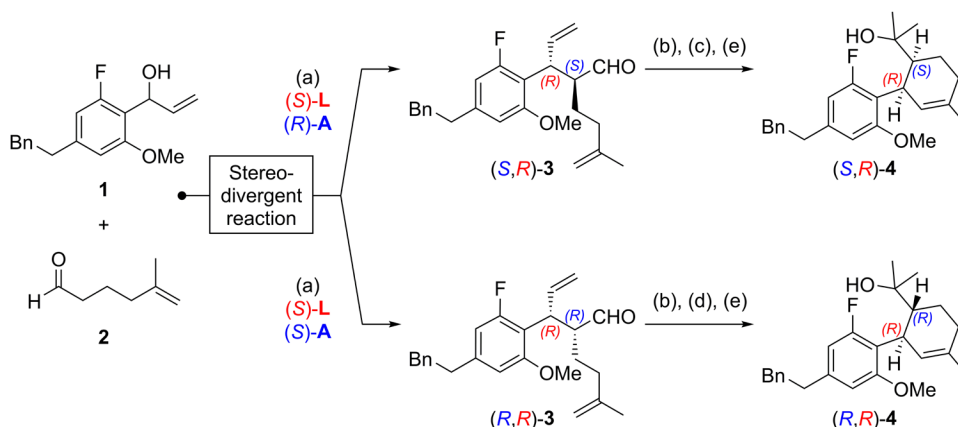

Fig. 2. Stereodivergent synthesis of S$_N$Ar precursors. Reagents and conditions: (a) 1.0 equiv **1**, 3.0 equiv **2**, 3 mol% [{Ir(cod)Cl}$_2$], 12 mol% (*S*)-L, 15 mol% (*S*)- or (*R*)-**A**, 5 mol% Zn(OTf)$_2$, 1,2-dichloroethane (0.5 M), 25°C, 20 hours, for (*S*,*R*)-**3**: 59% yield, > 20:1 diastereomeric ratio (d.r.), >99% enantiomeric excess (e.e.), for (*R*,*R*)-**3**: 76% yield, > 12:1 d.r., >99% e.e.; (b) 5 mol% Grubbs II cat., CH$_2$Cl$_2$, 25°C, 16 hours; (c) 2.3 equiv NaClO$_2$, 2.0 equiv NaH$_2$PO$_4$, 30 equiv 2-methyl-2-butene, *tert*-BuOH/H2O, 25°C; then 2.0 equiv Me$_3$SiCHN$_2$, C$_6$H$_6$/MeOH, 0°C, 90 min; (d) 8.0 equiv KOH, 3.9 equiv I$_2$, MeOH, 0°C, 45 min; (e) 4.0 equiv MeMgBr, THF, 25°C, for (*S*,*R*)-**4**: 56% yield over three steps, for (*R*,*R*)-**4**: 56% yield over three steps; see the Supplementary Materials for structures of (*S*)-**L**, (*S*)-**A**, and (*R*)-**A**, as well as for further details.
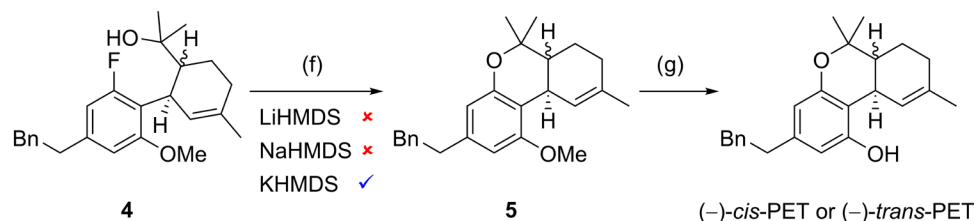
Fig. 3. Stereodivergent total synthesis of (−)-*cis*-PET and (−)-*trans*-PET. Reagents and conditions: (f) 1.6 equiv KHMDS, THF, 65°C, 15 hours, for (*S,R*)-**5**: 78% yield, (*R,R*)-**5**: 82% yield; (g) 10.0 or 20.0 equiv NaSEt, DMF, 140°C, 16 hours, for (−)-*cis*-PET: 80% yield, (−)-*trans*-PET: 83% yield.

The outcome of the crucial S_NAr cyclization was highly dependent on the choice of base; in reactions with LiHMDS and NaHMDS, the substrate proved to be unreactive, with full recovery of starting material after 16 hours in refluxing tetrahydrofuran (THF). The use of KHMDS under otherwise identical conditions resulted in the formation of (*S,R*)-**5** and (*R,R*)-**5** in high yield (Fig. 3). Last, demethylation with sodium ethanethiolate in *N,N'*-dimethylformamide (DMF) at 140°C afforded (−)-*cis*-PET and (−)-*trans*-PET.

In vitro pharmacology of PET and Δ^9-THC isomers on cannabinoid receptors and endocannabinoid-degrading enzymes

At the human cannabinoid receptor type 1 (CB1R), the natural product *cis*-PET exhibited a K_i = 481 nM, while its diastereoisomer *trans*-PET was more potent (K_i = 127 nM) (see Table 1 and fig. S1). Similarly, at the human peripheral cannabinoid receptor type 2 (CB2R), K_i values of 225 and 126 nM for *cis*- and *trans*-PET were measured, respectively. These differences parallel the lower affinity of Δ^9-*cis*-THC compared to Δ^9-*trans*-THC. Δ^9-*cis*-THC is a minor cannabinoid in cannabis (*16*) and a moderately active CB1R partial agonist (Table 1), in agreement with the in vivo data reported for racemic Δ^9-*cis*-THC prior to the identification of CB receptors (*17*). Thus, the benzyl substituent in PET does not fundamentally alter the binding relationships at CB receptors. In [^{35}S]GTPγS binding assays, both PETs were partial CB1R agonists such as the Δ^9-THCs, reaching 60 to 80% of the maximal efficacy of the known full CB1R/CB2R agonist CP55,940 (see Table 1 and fig. S2). At the CB1R functional level, *cis*-PET was about 10 times less potent than Δ^9-*trans*-THC [half maximal effective concentration (EC$_{50}$) = 406 nM versus 43 nM] (fig. S2A). Similarly, Δ^9-*trans*-THC showed a lower EC$_{50}$ value at CB2R compared with *cis*-PET (12 nM versus 167 nM) (fig. S2B). *cis*-PET was slightly more potent at CB2R than *trans*-PET, revealing a distinct stereochemical bias toward CB2R over CB1R at the functional level as compared with the corresponding Δ^9-THCs. At CB2R, all cannabinoids were inefficient partial agonists despite their nanomolar receptor binding affinities. No relevant effects on the major endocannabinoid-degrading enzymes fatty acid amid hydrolase (FAAH), monoacyl glycerol lipase (MAGL), and α/β hydrolases 6 and 12 (ABHD6 and ABHD12) were observed in vitro below 10 μM (table S1).

In vivo pharmacology of cis- and trans-PET

The potential cannabimimetic effects of PET diastereoisomers were assessed in vivo in a battery of four tests typically associated with CB1R activation in mice (hypothermia, catalepsy, hypolocomotion, and analgesia), collectively referred to as the "tetrad" (*14*). Experiments using various (i.e., equipotent to Δ^9-*trans*-THC) doses showed that *cis*-PET (50 mg/kg) and *trans*-PET (40 mg/kg) elicited the full

tetrad in BALB/c mice upon intraperitoneal injection (Fig. 4). The magnitude of hypothermia, catalepsy, hypolocomotion, and analgesia was in the same range as seen with Δ^9-*trans*-THC at the dose of 10 mg/kg, in agreement with the different potencies measured in vitro for CB1R activation. The pharmacological effects of PET and THC diastereoisomers were fully abolished by pretreatment with the CB1 receptor antagonist rimonabant (SR1) at 5 mg/kg, indicating that the tetrad is dependent on CB1 receptor activation in the brain.

LC-MS/MS quantification of cis- and trans-perrottetinene PET, endocannabinoids, prostaglandins, and arachidonic acid levels in mouse brain

We developed a liquid chromatography–tandem mass spectrometry (LC-MS/MS) method to quantify Δ^9-*trans*-THC, *cis*-PET, and *trans*-PET in the brain. Endocannabinoid levels and other *N*-acetylethanolamines (NAEs), arachidonic acid (AA), prostaglandin D$_2$ (PGD$_2$), and prostaglandin E$_2$ (PGE$_2$) were quantified to evaluate potential biochemical changes upon cannabinoid exposure (Fig. 5 and fig. S3). We measured Δ^9-*trans*-THC, *cis*-PET, and *trans*-PET concentrations of 0.24, 1.64, and 0.80 nmol/g, respectively, in total brain 1 hour after injection (Fig. 5A). This corresponds to a concentration of 197 nM for Δ^9-*trans*-THC, 1350 nM for *cis*-PET, and 662 nM for *trans*-PET, in line with the bioactive concentrations for CB1R activation (Table 1). Correlation between brain penetration and behavioral pharmacology was also observed for Δ^9-*trans*-THC (Fig. 5A), in line with the literature (*18*). In plasma, the concentrations of Δ^9-*trans*-THC, *cis*-PET, and *trans*-PET were 0.47, 1.79, and 1.56 nmol/ml, respectively (fig. S4). These results show that Δ^9-*trans*-THC and PET diastereoisomers rapidly and efficiently accumulate in the brain with C_{brain}/C_{plasma} ratios (K_p values) of 0.51 for Δ^9-*trans*-THC, 0.91 for *cis*-PET, and 0.51 for *trans*-PET. Animals treated with Δ^9-*trans*-THC, *cis*-PET, and *trans*-PET did not display any significant modulation of the endocannabinoids anandamide (AEA) and 2-arachidonoyl glycerol (2-AG) levels in the brain as compared with vehicle (Fig. 5, B and C). Similarly, the brain levels of AA were not affected by the treatments (Fig. 5D). Unexpectedly, *cis*- and *trans*-PET significantly reduced the basal levels of PGD$_2$ and PGE$_2$ in the brain in a CB1 receptor–dependent manner (Fig. 5, E and F). In sharp contrast, no significant acute effects on prostaglandins were observed in Δ^9-*trans*-THC–treated animals. Given the wide-reaching importance of prostaglandins in the brain (*19*, *20*), these pharmacological effects notably differentiate PET from Δ^9-*trans*-THC.

cis-PET pharmacology on major CNS targets

To characterize the in vitro pharmacology of *cis*-PET, we assessed this novel cannabinoid in a screening panel of 44 CNS targets, including G protein–coupled receptors (GPCRs), ion channels, nuclear

Table 1. Summary of binding interactions (K_i values) and functional activation ([^{35}S]GTPγS binding assay) of THC and PET diastereoisomers on human CB1R and CB2R. E_{max} values represent the maximal [^{35}S]GTPγS binding expressed as percentage of the vehicle-treated sample (100%). "Full" and "partial" in brackets stand for full and partial agonist.

| Cannabinoid	Receptor binding K_i values (nM, mean ± SD)		Receptor activation EC_{50} (nM) and E_{max} (%) values (mean ± SD)			
	CB1R	CB2R	CB1R (EC_{50})	CB1R (E_{max})	CB2R (EC_{50})	CB2R (E_{max})
CP55,940	1.2 ± 0.5	0.7 ± 0.3	17 ± 9	173 ± 6 (full)	1.9 ± 0.8	194 ± 5 (full)
Δ^9-*trans*-THC	22 ± 13	47 ± 11	43 ± 30	146 ± 3 (partial)	12 ± 7	134 ± 4 (partial)
Δ^9-*cis*-THC	228 ± 45	99 ± 29	552 ± 123	158 ± 6 (partial)	119 ± 69	153 ± 5 (partial)
trans-PET	127 ± 82	126 ± 55	171 ± 116	142 ± 5 (partial)	478 ± 288	116 ± 6 (partial)
cis-PET	481 ± 125	225 ± 61	406 ± 175	142 ± 5 (partial)	167 ± 136	113 ± 4 (partial)
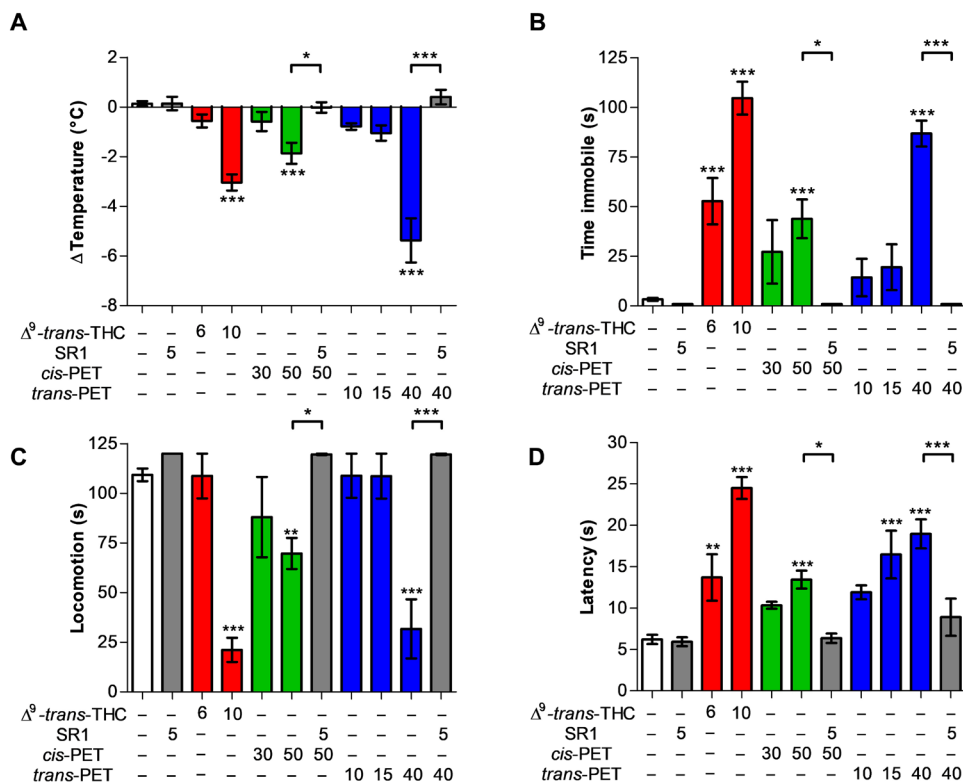
Fig. 4. CB1 receptor dependence of the pharmacological effects of Δ^9-*trans*-THC and PET diastereoisomers in mice. (**A**) Hypothermia, (**B**) catalepsy, (**C**) hypoloco-motion, and (**D**) analgesia elicited by Δ^9-*trans*-THC (red), *cis*-PET (green), and *trans*-PET (blue) compared with vehicle control (white) in BALB/c male mice 1 hour after intraperitoneal injection. The pharmacological effects were fully blocked by the CB1 receptor antagonist rimonabant (SR1, gray columns). Doses are expressed in mg/kg. Data show means ± SD. Groups were compared with the vehicle-treated control group using a one-way analysis of variance (ANOVA) following Tukey's post hoc test, n = 5 to 15 mice per group. ***$P < 0.001$, **$P < 0.01$, *$P < 0.05$ versus vehicle or as reported by the arches.

receptors, membrane transporters, and enzymes. At the concentration of 10 µM (blue line), *cis*-PET showed the highest binding affinity toward CB1R and CB2R (≥90%), followed by serotonin receptors 5-HT2A (86%) and 5-HT2B (85%), cholecystokinin receptor (CCK1; 84%), dopamine transporter (DAT; 83%), and ʟ-type Ca^{2+} channel (80%) (Fig. 6). At a concentration of 1 µM, *cis*-PET still binds significantly to CB1R (68%) and CB2R (75%), while it markedly lost

affinity for 5-HT2A (5%), 5-HT2B (30%), CCK1 (32%), DAT (27%), and ʟ-type Ca^{2+} channel (9%) (Fig. 6, orange line). This is in agreement with the full CB1R dependence of the *cis*-PET effects in vivo obtained in the behavioral tests (Fig. 4, tetrad) and modulation of prostaglandin levels in mouse brain (Fig. 5, E and F). Last, these data are also in perfect agreement with the measured brain concentration of *cis*-PET, which reached approximately 1.4 µM at the dose
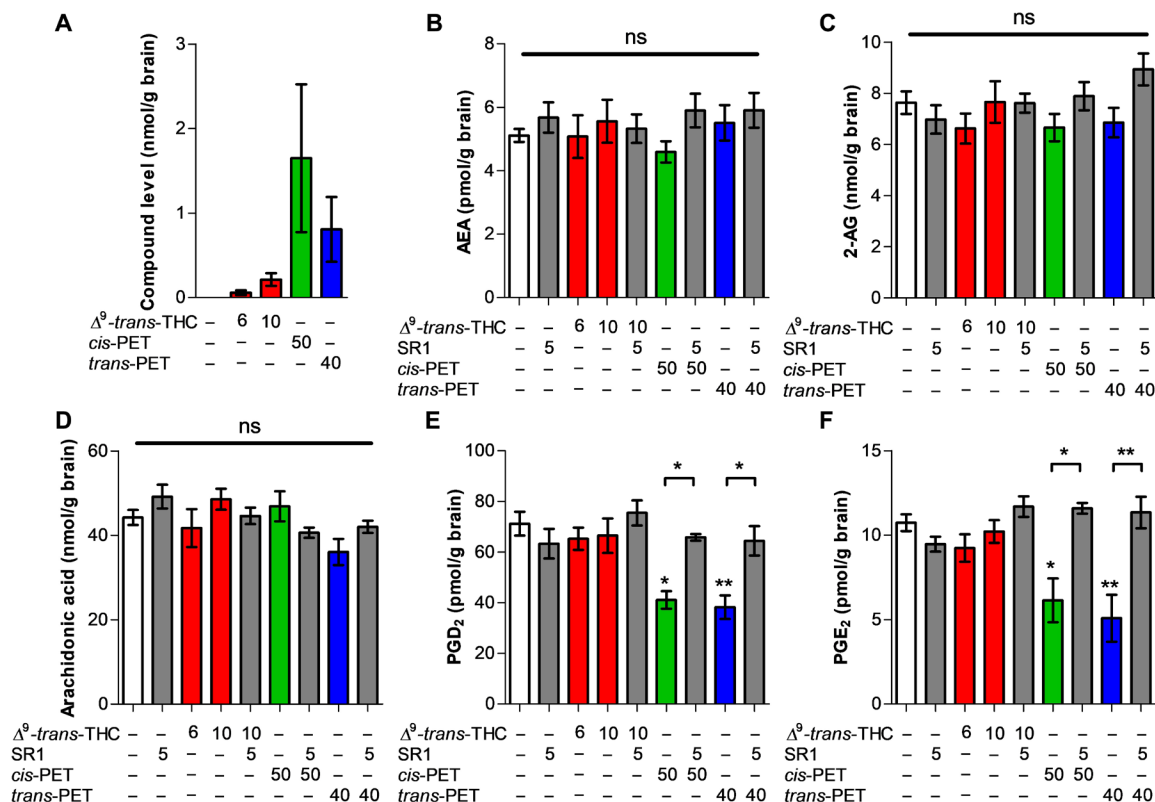
Fig. 5. Brain concentrations of Δ^9-*trans*-THC and PET diastereoisomers and induced biochemical changes. LC-MS/MS quantification of (**A**) Δ^9-*trans*-THC (red), *cis*-PET (green), and *trans*-PET (blue); (**B**) AEA; (**C**) 2-AG; (**D**) AA; (**E**) PGD$_2$; and (**F**) PGE$_2$ in the brain of male BALB/c mice 1 hour after intraperitoneal injection. The effects of PET diastereoisomers on PGD$_2$ and PGE$_2$ were inhibited by the CB1 receptor antagonist rimonabant (SR1). Doses are expressed in mg/kg. Data show means ± SD. Groups were compared with the vehicle-treated control group using a one-way ANOVA following Tukey's post hoc test $n = 5$ to 15 mice per group. **$P < 0.01$, *$P < 0.05$ versus vehicle or as reported by the arches. ns, not significant.

of 50 mg/kg (Fig. 5A). Δ^9-*trans*-THC has been shown to interact with other targets beyond CB receptors at concentrations between 1 and 10 μM, including 5-HT2A receptors, DAT, Ca^{2+} channels, Na$^+$ channels, Kv channels, and monoamino oxidase (MAO) (*21–23*). In addition, Δ^9-*trans*-THC inhibited 5-HT transporter (SERT) and norepinephrine transporter (NAT) at concentrations <1 μM (*21*, *22*). To directly compare *cis*-PET and Δ^9-*trans*-THC, the latter was also assessed in the screening panel of 44 CNS targets at 1 μM (Fig. 6). The results indicate specific binding to CB1R (95%) and CB2R (90%), with only minor effects on CCK1 (40%), DAT (22%), and histamine 1 receptor (H1; 20%). Neither Δ^9-*trans*-THC nor *cis*-PET inhibited cyclooxygenase-2 (COX-2) at physiological concentrations (Fig. 6 and fig. S5).

DISCUSSION

The isolation of the liverwort-derived bibenzyl cannabinoid *cis*-PET was first reported in 1994 (*5*), although in 1988 Crombie and co-workers already predicted *cis*-PET as a natural product (*24*). Possibly because of a lack of isolated pure substance, no research was conducted on its biological activity. In recent years, reports on *Radula* as legal high have accumulated. Our study shows that *cis*-PET is a moderately potent but efficacious psychoactive cannabinoid identified outside the *Cannabis* genus, in agreement with the reported recreational use of *R. marginata*, which is endemic to New Zealand

and Tasmania. Like Δ^9-*trans*-THC, *cis*-PET occurs in the plant as acid (*5*, *6*), which is progressively decarboxylated upon drying or smoking. Dried *R. marginata* collected in the wild is currently sold in the internet as legal high, making reference to *cis*-PET being structurally similar to THC (see Acknowledgments). The online community reporting about legal highs both affirms and refutes the anecdotes regarding the cannabis-like effects of smoked *R. marginata*. Given the uncertain amounts of *cis*-PET in the purchasable preparations and the lack of information regarding the pharmacology of *cis*-PET, we synthesized both PET diastereoisomers and tested them in vitro and in mice. We show that *cis*-PET is readily bioavailable to the brain in mice (K_p value of 0.91) and selectively binds to CB1 and CB2 cannabinoid receptors CB1R and CB2R at nanomolar concentrations in vitro, without affecting the other components of the ECS and 44 CNS targets including GPCRs, ion channels, nuclear receptors, membrane transporters, and enzymes. In vivo, *cis*-PET induced analgesia, catalepsy, hypolocomotion, and hypothermia (collectively called tetrad) in a CB1R-dependent manner similarly to Δ^9-*trans*-THC. As in the case of the THC scaffold, the *cis*-PET isomer is a less potent CB1R partial agonist than the *trans*-PET. Unexpectedly, the PET diastereoisomers differed pharmacologically from Δ^9-*trans*-THC as it significantly reduced basal PGD$_2$ and E$_2$ levels in the brain in a CB1R-dependent manner, potentially limiting its adverse effects (*20*) and reducing neuroinflammation (*19*, *25*). The interplay between CB1R activation by cannabinoids
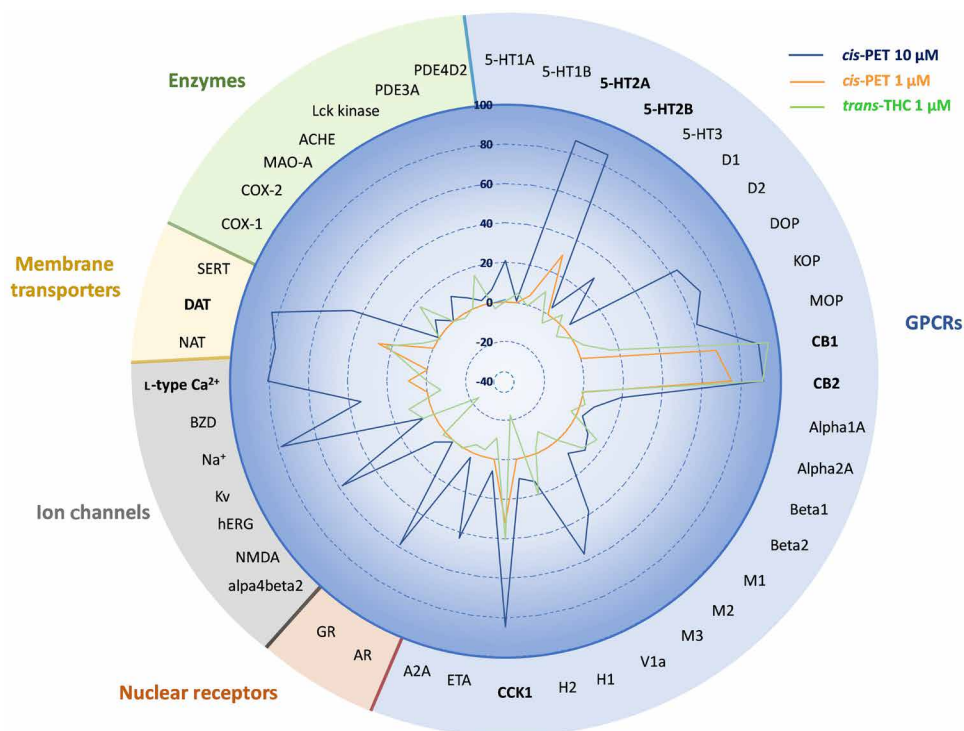
Fig. 6. Effects of *cis*-PET and Δ^9-*trans*-THC on a panel of 44 CNS targets (GPCRs, ion channels, nuclear receptors, membrane transporters, and enzymes). Data show the percentage of binding or protein activity (enzyme, transporter, and ion channels) at test concentrations of 10 μM (*cis*-PET, blue line) and 1 μM (*cis*-PET, orange line; Δ^9-*trans*-THC, green line). Data presented are obtained from two independent experiments each performed in duplicate. For full names of abbreviations, see the Supplementary Materials. The 100% is intended as full enzymatic activity (enzymes), substrate transport (membrane transporter), receptor binding (GPCRs and nuclear receptors), and ion permeability (ion channels). The percentage is expressed as positive or negative values based on an increase or reduction of the target protein.

and modulation of PGE$_2$ has been emphasized previously. Activation of CB1R by Δ^9-*trans*-THC and CP55,940 was shown to induce COX-2 expression in different cell types, including neurons and astrocytes (*20*, *26*, *27*). Chen and colleagues (*20*) reported that Δ^9-*trans*-THC acutely increases COX-2 expression in the brain in a CB1R-dependent mechanism by specifically recruiting a Gβγ subunit–mediated intracellular signaling, while 2-AG led to CB1R-dependent COX-2 suppression via the Gα$_i$ subunit. Moreover, in vivo, Δ^9-*trans*-THC (10 mg/kg) strongly increased basal PGE$_2$ levels in the hippocampal region, giving rise to central adverse effects (*20*). Using the same dose of Δ^9-*trans*-THC, in our experiments we could not detect a significant change of basal PGD$_2$ and PGE$_2$ levels in mouse whole brain (Fig. 5, E and F). Conversely, PET diastereomers specifically reduced basal PGD$_2$ and PGE$_2$ levels without affecting COX-2 activity. It remains to be determined whether PET recruits the CB1R-mediated transduction pathways reported for 2-AG, which also reduces basal prostaglandin levels (*19*, *28*). Recent studies have provided strong evidence that low-dose Δ^9-*trans*-THC treatment may still be beneficial with reduced central side effects (*29*, *30*). Thus, the less potent PET diastereoisomers showing additional effects on brain prostaglandin levels exhibit pharmacological characteristics of potential medical phytocannabinoids. The inhibition of constitutive prostaglandin production is not associated with toxic effects in the brain, while in the periphery, it may induce an impairment of the renal plasma flow, possibly leading to kidney injury (*31*–*33*). Although the moderate but significant inhibition of brain prostaglandin levels induced by *cis*-PET is not comparable to the

pharmacological blockage of COX-2 activity elicited by nonsteroidal anti-inflammatory drugs, the reduction of brain prostaglandins may contribute to the neuropharmacology of this new cannabinoid (*20*). Our data also provide additional important information about the functional consequences of Δ^9-THC side-chain modifications (*34*, *35*). Using stereodivergent total synthesis, after more than 20 years from the first report of *cis*-PET, this study finally uncovers the underlying molecular mechanism of action. This gives a rationale for the recreational use of *Radula* liverworts and provides a molecular basis on which to assess the prospective toxicity and usefulness of the plant material.

Moreover, the findings on the pharmacological effects of *cis*-PET provide a marked example of convergent evolution of bioactive plant secondary metabolites in the plant kingdom. Despite the existence of more than 20,000 bryophyte species globally, *cis*-PET is the first psychoactive constituent in this group of plants. Recently, putative genes involved in the biosynthesis of *cis*-PET were described (*8*). The abuse potential of *Radula* species is probably low, given the relatively moderate potency and low abundance of *cis*-PET (0.7 to 7% in an extract) (*5*, *6*) as compared with marijuana, with Δ^9-*trans*-THC contents typically higher than 10% (*36*). Nevertheless, *cis*-PET could be an interesting lead for drug development as it might have fewer side effects than Δ^9-*trans*-THC and reduces prostaglandins. The likely relevance of signaling-specific CB1R pathways (*37*), in particular related to the reduced prostaglandin biosynthesis observed with the bibenzyl PET scaffold, will need to be studied in preclinical disease models.

MATERIALS AND METHODS

General

Unless otherwise noted, all reactions were carried out under an ambient atmosphere, and all reagents were purchased from commercial suppliers and used without further purification. The amine catalysts (S)-α,α-bis[3,5-bis(trifluoromethyl)phenyl]-2-pyrrolidinemethanol trimethylsilyl ether and (R)-α,α-bis[3,5-bis(trifluoromethyl)phenyl]-2-pyrrolidinemethanol trimethylsilyl ether were purchased from Sigma-Aldrich. The (R)-enantiomer was received as an off-white solid and was therefore purified by column chromatography before use to give a white solid. [Ir(cod)Cl]$_2$ (97%) was purchased from Combi-Blocks Inc. Analytical thin-layer chromatography (TLC) was performed on Merck silica gel 60 F254 TLC glass plates and visualized with 254-nm light and potassium permanganate or Seebach's "magic" staining solutions followed by heating. Purification of reaction products was carried out by flash chromatography using Sigma-Aldrich silica gel, 60 Å, 230 to 400 mesh under 0.3 to 0.5 bar pressure. The ligands (S)-**L** and achiral rac-**L** were prepared following known procedures (13, 38). Aldehyde **2** was prepared by published procedures (13, 39). ^{1}H nuclear magnetic resonance (NMR) spectra were recorded on a Bruker AV 400-MHz spectrometer and are reported in parts per million (ppm), with the solvent resonance used as the internal standard (CHCl$_3$ at 7.26 ppm). Peaks are reported as follows: s = singlet, d = doublet, t = triplet, q = quartet, or m = multiplet, coupling constant(s) in Hz, integration. ^{13}C NMR spectra were recorded with ^{1}H decoupling on a Bruker AV 101-MHz or Bruker AV 151-MHz spectrometer and are reported in parts per million, with the solvent resonance used as the internal standard (CDCl$_3$ at 77.16 ppm). Peaks are reported as follows: s = singlet, d = doublet, coupling constant(s) in Hz. ^{19}F NMR spectra were recorded with ^{1}H decoupling on a Bruker AV 377-MHz or Bruker AV 471-MHz spectrometer and are reported in parts per million. Peaks are reported as follows: s = singlet, d = doublet, coupling constant(s) in Hz. Unless otherwise noted, all NMR measurements were conducted at room temperature. NMR service measurements were obtained at the NMR spectrometry service operated by the Laboratory of Organic Chemistry at the Eidgenössische Technische Hochschule Zürich (ETHZ). Infrared spectra were measured neat on a PerkinElmer UATR Two Spectrometer. The peaks are reported as absorption maxima (n, cm^{-1}). High-resolution mass spectral data were obtained at the MS service operated by the Laboratory of Organic Chemistry at the ETHZ on a Micromass (Waters) AutoSpec Ultima–EI-Sector-MS (EI), Bruker maXis–ESI-Qq-TOF-MS (ESI), or Bruker solariX–MALDI-FTICR-MS (Dual MALDI/ESI) and are reported as mass/charge ratio (m/z). Enantiomeric excesses were determined on a Waters ACQUITY UltraPerformance Convergence Chromatography supercritical fluid chromatography (SFC) system using a chiral stationary phase DAICEL CHIRALCEL OJ-H (3 μm, 4.6 mm by 150 mm). Optical rotations were measured with a JASCO P-2000 Polarimeter (10 cm, 1-ml cell).

Chemicals

[^{3}H]CP55,940 and [^{35}S]GTPγS were obtained from PerkinElmer Life Sciences (Waltham, MA, USA). WIN55,212, AA (5Z,8Z,11Z,14Z-eicosatetraenoic acid), AA-d8 (5Z,8Z,11Z,14Z-eicosatetraenoic-5,6,8,9,11,12,14,15-d8 acid), AEA (N-(2-hydroxyethyl)-5Z,8Z,11Z,14Z-eicosatetraenamide), AEA-d4 [N-(2- hydroxyethyl-1,1,2,2-d4)-5Z,8Z,11Z,14Z-eicosatetraenamide], 2-AG (5Z,8Z,11Z,14Z-eicosatetraenoic acid, 2-glyceryl ester), 2-AG-d5 (5Z,8Z,11Z,14Z-eicosatetraenoic acid, 2-glyceryl-1,1,2,3,3-d5 ester), linoleoyl ethanolamide [LEA or

N-(2-hydroxyethyl)-9Z,12Z-octadecadienamide], LEA-d4 [N-(2-hydroxyethyl-1,1,2,2-d4)-9Z,12Z-octadecadienamide], oleoyl ethanolamide [OEA or N-(2-hydroxyethyl)-9Z-octadecenamide], OEA-d4 [N-(2-hydroxyethyl-1,1,2,2-d4)-9Z-octadecenamide], palmitoylethanolamide [PEA or N-(2-hydroxyethyl)-hexadecanamide], PEA-d5 [N-(2-hydroxyethyl)-hexadecanamide-15,15,16,16,16-d5], PGE$_2$ (9-oxo-11α,15S-dihydroxy-prosta-5Z,13E-dien-1-oic acid), PGE$_2$-d4 (9-oxo-11α,15S-dihydroxy-prosta-5Z,13E-dien-1-oic-3,3,4,4-d4 acid), PGD$_2$ (9α,15S-dihydroxy-11-oxo-prosta-5Z,13E-dien-1-oic acid), progesterone (PROG or 4-pregnene-3,20-dione), PROG-d9 (progesterone-2,2,4,6,6,17α,21,21,21-d9), and corticosterone (11β,21-dihydroxy-pregn-4-ene-3,20-dione) were obtained from Cayman Chemicals Europe (Ann Arbor, MI, USA). Guanosine triphosphate (GTP) and guanosine diphosphate (GDP) were purchased from Sigma (St. Louis, Missouri, USA). Rimonabant (SR141716A, SR1) with a purity >98% was ordered from Pharmaserv AG, Switzerland. (−)-Δ^9-cis-THC and (−)-Δ^9-trans-THC were synthesized and prepared with a purity >95% as previously reported (see the Supplementary Materials for NMR spectra) (13).

Radioligand binding assays on cannabinoid receptors

The assay was performed as previously described (40). Briefly, 15 μg of membrane preparation obtained from CHO cells stably transfected with hCB$_1$ or hCB$_2$ receptors were resuspended in 300 μl of binding buffer [50 mM tris-HCl, 2.5 mM EDTA, 5 mM MgCl$_2$, and fatty acid–free bovine serum albumin (BSA; 0.5 mg/ml) (pH 7.4)] in silanized glass tubes and coincubated with the tested compounds at different concentrations (1 pM to 100 μM) or vehicle and 0.5 nM [^{3}H]CP55,940 (168 Ci/mmol) for 1.5 hours at 30°C. Nonspecific binding of the radioligand was determined in the presence of 10 μM WIN55,512. After the incubation time, membrane suspensions were rapidly filtered through a 0.5% polyethyleneimine presoaked 96-well microplate bonded with GF/B glass fiber filters (UniFilter-96 GF/B, PerkinElmer Life Sciences) under vacuum and washed 12 times with 150 μl of ice-cold washing buffer. Filters were added to 45 μl of MicroScint-20 scintillation liquid, and radioactivity was measured with the 1450 MicroBeta Trilux top counter. Data were collected from at least three independent experiments performed in triplicate, and the nonspecific binding was subtracted. Results were expressed as [^{3}H]CP55,940 bound as percentage of binding in vehicle-treated samples, and K$_i$ (inhibition constant) values were calculated applying the Cheng-Prusoff equation.

[^{35}S]GTPγS binding assay

The assay was performed as previously described (40). Briefly, 5 μg of clean membrane prepared in-house from CHO-hCB2 and CHO-hCB1 cells was diluted in silanized plastic tubes with 200 μl of GTPγS binding buffer [50 mM tris-HCl, 3 mM MgCl$_2$, 0.2 mM EGTA, and 100 mM NaCl (pH 7.4) supplemented with 0.5% of fatty acid–free BSA] in the presence of 10 μM GDP and 0.1 nM [^{35}S]GTPγS (1250 Ci/mmol). The mixture was kept on ice until the binding reaction was started by adding the tested compound, vehicle (negative control), or CP55,940 (positive control). Nonspecific binding was measured in the presence of 10 μM GTPγS (Sigma). The tubes were incubated at 30°C for 90 min under shaking, and then, they were put on ice to stop the reaction. An aliquot (185 μl) of the reaction mixture was rapidly filtered through a 96-well microplate bonded with GF/B glass fiber filters (UniFilter-96 GF/B, PerkinElmer Life Sciences) previously presoaked with ice-cold washing buffer [50 mM

tris-HCl (pH 7.4) plus of 0.1% fatty acid–free BSA]. The filters were washed six times with 180 μl of washing buffer under vacuum and dried under the air drier flow. The radioactivity was measured with the 1450 Microbeta WallacTrilux Top counter after the addition of 45 μl of scintillation cocktail. Specific binding was calculated by subtracting the residual radioactivity signal obtained in presence of an excess of GTPγS, and the results were expressed as percentage of vehicle control.

Enzyme inhibition assays for FAAH, MAGL, ABHD6, ABHD12, and COX-2

The enzyme inhibition assays were performed as previously published (40). Briefly, for AEA and 2-OG hydrolysis, different concentrations of cis-PET, trans-PET, and Δ^9-trans-THC were preincubated with 200 μg of pig brain homogenate in tris-HCl buffer (pH 7.6) supplemented with 0.1% of fatty acid–free BSA for 20 min at 37°C. Then, 0.1 μM AEA or 1 μM 2-OG containing trace amounts of [ethanolamine-1-3H]-AEA (1 nM) or [glycerol-1,2,3-3H]-2-OG (1 nM), respectively, were incubated with the mixtures for another 15 min at 37°C. The reaction was stopped by adding two volumes of ice-cold CHCl₃:MetOH mixture (1:1) and centrifuged at 16,000g for 10 min at 4°C. The aqueous phase was collected, and the radioactivity was measured by liquid scintillation spectroscopy. hABHD6 and hABHD12 activity was determined using cell homogenates from hABHD6 and hABHD12 stably transfected human embryonic kidney (HEK) 293 cells. Different concentrations of cis-PET, trans-PET, and Δ^9-trans-THC were preincubated with 40 μg of cell homogenate for 30 min at 37°C in assay buffer [1 mM tris, 10 mM EDTA, and 0.1% BSA (pH 7.6)]. Dimethyl sulfoxide (DMSO) was used as vehicle control, and 10 μM WWL70 or 20 μM tetrahydrolipstatin (THL) as positive controls. Then, 10 μM 2-OG was added and incubated for 5 min at 37°C. The reaction was stopped by the addition of 400 μl of ice-cold CHCl₃:MeOH (1:1). The samples were vortexed and centrifuged (16,000g, 10 min, 4°C). Aliquots (200 μl) of the aqueous phase were assayed for tritium content by liquid scintillation spectroscopy. Blank values were recovered from tubes containing no enzyme. Basal 2-OG hydrolysis occurring in nontransfected HEK293 cells was subtracted. Inhibition of human recombinant COX-2 was assessed using an in-house validated COX fluorescent inhibitor screening assay kit from Cayman Chemical Europe as previously described (40).

In vitro pharmacological screening

cis-PET and Δ^9-trans-THC were profiled in a Cerep (Eurofins Pharma Discovery Services) screening panel of 44 targets including GPCRs, ion channels, nuclear receptors, membrane transporters, and enzymes mostly expressed in the CNS. cis-PET was tested at 1 and 10 μM, while Δ^9-trans-THC was tested only at 1 μM. Data presented were obtained from two independent experiments each performed in duplicate. The GPCRs tested were as follows: α₁A adrenergic receptor, α₂A adrenergic receptor, α₂B adrenergic receptor, β₁ adrenergic receptor, β₂ adrenergic receptor, CB1R, CB2R, D1 dopamine receptor type 1, D2 dopamine receptor type 2, H1 histamine receptor type 1, H2 histamine receptor type 2, delta-type opioid receptor, mu-type opioid receptor, kappa-type opioid receptor, 5-HT1A serotonin receptor, 5-HT1B serotonin receptor, 5-HT2A serotonin receptor, 5-HT2B serotonin receptor, 5-HT3 serotonin receptor, M1 muscarinic receptor, M2 muscarinic receptor, M3 muscarinic receptor, A2A adenosine receptor, ETA endothelin receptor, CCK1 cholecystokinin A receptor, and V1A vasopressin/

oxytocin receptor. Ion channels were as follows: GABAA channel at the benzodiazepine (BZD), α4/β2 acetylcholine ion channel, Cav1.2 (L-type) calcium ion channel (dihydropyridine site), Kv voltage-gated potassium ion channel, Na+ voltage-gated sodium channel, human ether-a-go-go–related gene (hERG) potassium channels, N-methyl-D-aspartate (glutamate) receptor. Nuclear receptors were as follows: androgen receptor and glucocorticoid receptor. Enzymes were as follows: MAO-A, acetylcholinesterase, lymphocyte-specific protein tyrosine kinase phosphodiesterase 3A, phosphodiesterase 4D2, COX-1, and COX-2. Membrane neurotransmitter transporters were as follows: noradrenaline transporter, DAT, and serotonin transporter.

Animals

In vivo experiments were performed in accordance with the Swiss Federal guidelines, which agree with the Institutional Animal Care and Use Committee (IACUC) guidelines. Male BALB/c mice (8 to 10 weeks old) were provided by Janvier Labs (St Berthevin, France). Mice were housed in groups of five per cage in a specific pathogen–free unit under controlled 12-hour light/12-hour dark cycle (ambient temperature, 21° ± 2°C; humidity, 40 to 50%) with free access to standard rodent chow and water. The mice were acclimatized to the animal house for 1 week before the experiments.

Tetrad test

Compounds were dissolved in pure DMSO and administered intraperitoneally at different doses using five to eight mice for each treatment group. cis-PET, trans-PET, and Δ^9-trans-THC were administered 1 hour before assessing locomotion, catalepsy, body temperature, and analgesia (collectively referred as tetrad test). The rectal temperature was measured before (basal) and 1 hour after injection with a thermocouple probe (1 to 2 cm; Testo AG, Switzerland), and the change in rectal temperature was expressed as the difference between basal and postinjection temperatures. Catalepsy was measured using the bar test, where mice were retained in an imposed position with forelimbs resting on a bar 4 cm high; the end point of catalepsy was considered when both front limbs were removed or remained over 120 s. Locomotion was determined using the rotarod test; animals were placed on the rotarod (Ugo Basile, Italy) at 6 rpm, and the latency to fall was measured with a cutoff time of 120 s. Catalepsy and locomotion were measured in three trials. The hot plate test was performed to evaluate analgesia using a 54° to 56°C hot plate (Thermo Scientific, Waltham, Massachusetts, USA) with a Plexiglas cylinder. The latency to the first nociceptive response (paw lick or foot shake) was measured.

LC-MS/MS quantifications of PET, THC, AEA, 2-AG, PEA, LEA, OEA, AA, PGD₂, and PGE₂ in mouse brain tissue

LC-MS/MS analyses were performed on a Shimadzu UFLC coupled to a TripleQuad 4000 QTRAP mass spectrometer (ABSciex Concord, Ontario, Canada). AEA, 2-AG, OEA, PEA, LEA, AA, PGE₂, and PGD₂ were quantified in mouse brains using our recently published method (40). For the analysis of cis-PET, trans-PET, and Δ^9-trans-THC, a Reprosil Fluosil 100 PFP (particle size, 3 μm; 2 mm by 50 mm; Dr. A. Maisch, Germany) column was used in reversed-phase mode with gradient elution starting with 95% of phase A (0.1% formic acid and 2 mM ammonium acetate in water) and 5% of phase B (0.1% formic acid in acetonitrile). The amount of phase B was linearly increased to 40% at 3 min, then to 58% at 8 min and kept for 1 min, and then increased linearly again to 80% at 10 min;

the column was flushed for 3.5 min with 99% of phase B with subsequent reequilibration at 5% for a further 3 min. The total analysis time was 17 min at 40°C, the flow rate was 0.3 ml/min, and the injection volume was 10 μl. These LC conditions provided the chromatographic resolution of *cis*- and *trans*-PET prior to MS/MS (see fig. S6 for the chromatogram), where both isomers ([M+H+] of 349 *m/z*) showed the same fragmentation pattern (*m/z* = 293, 267, 227). The TurboIon Spray interface was operated in positive mode. The MS parameters of the ESI source were as follows: capillary voltage, 4.5 kV; temperature, 600°C; nebulizer pressure, 50 psi. Peaks were integrated using the Analyst software version 1.5 (AB Sciex Concord, Ontario, Canada). Because of the lack of a deuterated version for interested molecules and the chemical similarity between Δ^9-*trans*-THC and both PET isomers, we used Δ^9-*trans*-THC as internal standard (IS) for *cis*- and *trans*-PET, whereas *cis*-PET was used as IS for Δ^9-*trans*-THC. The ratio of peak area of analyte to peak area of IS was used to ensure linearity of the calibrations. The slope, intercept, and regression coefficient of those calibration lines were determined. The concentrations of PET diastereosimoners and Δ9-*trans*-THC in the brain and plasma were calculated applying a model previously described (*40*). The ratios between brain and plasma concentrations (K_p) of Δ^9-*trans*-THC, *cis*-PET, and *trans*-PET were calculated as previously reported (*40*).

Sample preparation

Mouse brains were divided into two sagittal hemispheres, and one hemisphere was used for LC-MS/MS analyses. Half brains were weighted when still frozen and transferred to 2-ml microcentrifuge vials (XXTuff Microvials, BioSpec, Oklahoma, USA) with three chrome-steel beads (diameter, 2.3 mm; BioSpec, Oklahoma, USA) and 1.5 ml of 0.1 M formic acid. Samples were homogenized using a 24-position Mini bead beater (BioSpec Products Inc., Bartlesville, OK, USA) for the extraction of administered molecules (*cis*-PET, *trans*-PET, and Δ9-*trans*-THC), as well as for endogenous molecules AEA, 2-AG, PEA, OEA, LEA, PGE₂, PGD₂, AA, corticosterone, and progesterone using a previously described extraction protocol (*40*). For the quantification of *cis*-PET, *trans*-PET, and Δ^9-*trans*-THC, a different extraction method was used. Briefly, 200 μl of brain homogenate or plasma was rapidly transferred to a silanized Eppendorf tube containing 400 μl of acetone and 400 ng/ml of the designed internal standard. Samples were centrifuged at 13,200 rpm for 10 min at 4°C to precipitate proteins, and the supernatant was further extracted with 1 ml of ethyl acetate:hexane (9:1) 0.1% formic acid strongly vortexed for 30 s and sonicated (Sonicator Merck-Gruppe) in a cold bath for 5 min. Samples were centrifuged at 13,200 rpm for 10 min at 4°C and kept for 1 hour at −20°C to freeze the lower aqueous phase. The upper organic phase was recovered in plastic tubes and dried into a speed vacuum. The extracts were reconstituted in 50 μl of acetonitrile with 20% of water, and 10 μl was injected in the LC-MS/MS system.

Statistical analyses

Data were collected from at least three independent experiments each performed in triplicate. Results are expressed as mean values and standard error deviation. The statistical significance difference among groups was determined by the Student's *t* test (paired, one-tailed, or two-tailed *t* test) or one-way ANOVA followed by a Tukey's post hoc test. Statistical differences between the treated and control groups were considered as significant if $p \leq 0.05$. GraphPad 5.0

software was used to fit the concentration-dependent curves and for the statistical analysis.

SUPPLEMENTARY MATERIALS

Supplementary material for this article is available at http://advances.sciencemag.org/cgi/content/full/4/10/eaat2166/DC1

Fig. S1. Radioligand displacement assay using [³H]CP55,940 and membranes from CHO cells stably transfected with human CB1R and CB2R, respectively.
Fig. S2. [³⁵S]GTPγS binding curves for THC and PET stereoisomers on human cannabinoid receptors.
Fig. S3. LC-MS/MS quantifications of the NAEs OEA, PEA, and LEA in the brain of BALB/c male mice 1 hour after intraperitoneal injection of cannabinoids.
Fig. S4. LC-MS/MS quantification of Δ9-*trans*-THC, *cis*-PET, and *trans*-PET in plasma of BALB/c male mice 1 hour after intraperitoneal injection of cannabinoids.
Fig. S5. Inhibition of COX-2 activity.
Fig. S6. Representative LC-MS/MS reaction monitoring chromatogram of reference standards in mouse brain tissue showing LC separation of *cis*- and *trans*-PET.
Table S1. Profiling of THC and PET diastereoisomers on endocannabinoid-degrading enzymes in vitro.
Synthesis and characterization of products
Preparation of allylic alcohol 1
Preparation of (–)-*cis*-PET [(*S,R*)-PET]
Preparation of (–)-*trans*-PET [(*R,R*)-PET]
SFC traces

REFERENCES AND NOTES

1. R. Mechoulam, L. O. Hanuš, R. G. Pertwee, A. C. Howlett, Early phytocannabinoid chemistry to endocannabinoids and beyond. *Nat. Rev. Neurosci.* **15**, 757–764 (2014).
2. E. B. Russo, History of cannabis and its preparations in saga, science, and sobriquet. *Chem. Biodivers.* **4**, 1614–1648 (2007).
3. Y. Gaoni, R. Mechoulam, Isolation, structure, and partial synthesis of an active constituent of Hashish. *J. Am. Chem. Soc.* **86**, 1646–1647 (1964).
4. J. Gertsch, R. G. Pertwee, V. Di Marzo, Phytocannabinoids beyond the *Cannabis* plant—Do they exist? *Br. J. Pharmacol.* **160**, 523–529 (2010).
5. M. Toyota, T. Kinugawa, Y. Asakawa, Bibenzyl cannabinoid and bisbibenzyl derivative from the liverwort *Radula perrottetii*. *Phytochemistry* **37**, 859–862 (1994).
6. M. Toyota, T. Shimamura, H. Ishii, M. Renner, J. Brag-gins, Y. Asakawa, New bibenzyl cannabinoid from the New Zealand liverwort *Radula marginata*. *Chem. Pharm. Bull.* **50**, 1390–1392 (2002).
7. F. Cullman, H. Becker, Prenylated bibenzyls from the liverwort *Radula laxiramea*. *Z. Naturforsch.* **54**, 147–150 (1999).
8. T. Hussain, B. Plunkett, M. Ejaz, E. V. Espley, O. Kayser, Identification of putative precursor genes for the biosynthesis of cannabinoid-like compound in *Radula marginata*. *Front. Plant Sci.* **9**, 537 (2018).
9. Y. Asakawa, A. Ludwiczuk, Chemical constituents of bryophytes: Structures and biological activity. *J. Nat. Prod.* **81**, 641–660 (2018).
10. Y. Song, S. Hwang, P. Gong, D. Kim, S. Kim, Stereoselective total synthesis of (–)-perrottetinene and assignment of its absolute configuration. *Org. Lett.* **10**, 269–271 (2008).
11. S. Krautwald, D. Sarlah, M. A. Schafroth, E. M. Carreira, Enantio- and diastereodivergent dual catalysis: α-Allylation of branched aldehydes. *Science* **340**, 1065–1068 (2013).
12. S. Krautwald, M. A. Schafroth, D. Sarlah, E. M. Carreira, Stereodivergent α-allylation of linear aldehydes with dual iridium and amine catalysis. *J. Am. Chem. Soc.* **136**, 3020–3023 (2014).
13. M. A. Schafroth, G. Zuccarello, S. Krautwald, D. Sarlah, E. M. Carreira, Stereodivergent total synthesis of Δ⁹-tetrahydrocannabinols. *Angew. Chem. Int. Ed.* **53**, 13898–13901 (2014).
14. K. Monory, H. Blaudzun, F. Massa, N. Kaiser, T. Lemberger, G. Schütz, C. T. Wotjak, B. Lutz, G. Marsicano, Genetic dissection of behavioural and autonomic effects of Δ⁹-tetrahydrocannabinol in mice. *PLOS Biol.* **5**, e269 (2007).
15. M. V. Westphal, M. A. Schafroth, R. C. Sarott, M. A. Imhof, C. P. Bold, P. Leippe, A. Dhopeshwarkar, J. M. Grandner, V. Katritch, K. Mackie, D. Trauner, E. M. Carreira, J. A. Frank, Synthesis of photoswitchable Δ⁹-tetrahydrocannabinol derivatives enables optical control of cannabinoid receptor 1 signaling. *J. Am. Chem. Soc.* **139**, 18206–18212 (2017).
16. R. M. Smith, K. D. Kepfert, Δ¹-3,4-Cis-tetrahydrocannabinol in *Cannabis sativa*. *Phytochemistry* **16**, 1088–1089 (1977).
17. D. B. Uliss, H. C. Dalzell, G. R. Handrick, J. F. Howes, R. K. Razdan, Hashish. Importance of the phenolic hydroxyl group in tetrahydrocannabinols. *J. Med. Chem.* **18**, 213–215 (1975).
18. A. S. Spiro, A. Wong, A. A. Boucher, J. C. Arnold, Enhanced brain disposition and effects of Δ⁹-tetrahydrocannabinol in P-glycoprotein and breast cancer resistance protein knockout mice. *PLOS ONE* **7**, e35937 (2012).

19. D. K. Nomura, B. E. Morrison, J. L. Blankman, J. Z. Long, S. G. Kinsey, M. C. G. Marcondes, A. M. Ward, Y. K. Hahn, A. H. Lichtman, B. Conti, B. F. Cravatt, Endocannabinoid hydrolysis generates brain prostaglandins that promote neuroinflammation. *Science* **334**, 809–813 (2011).

20. R. Chen, J. Zhang, N. Fan, Z.-Q. Teng, Y. Wu, H. Yang, Y.-P. Tang, H. Sun, Y. Song, C. Chen, Δ^9-THC-caused synaptic and memory impairments are mediated through COX-2 signaling. *Cell* **155**, 1154–1165 (2013).

21. R. G. Pertwee, The diverse CB_1 and CB_2 receptor pharmacology of three plant cannabinoids: Δ^9-Tetrahydrocannabinol, cannabidiol and Δ^9-tetrahydrocannabivarin. *Br. J. Pharmacol.* **153**, 199–215 (2008).

22. X. Viñals, E. Moreno, L. Lanfumey, A. Cordomí, A. Pastor, R. de La Torre, P. Gasperini, G. Navarro, L. A. Howell, L. Pardo, C. Lluís, E. I. Canela, P. J. McCormick, R. Maldonado, P. Robledo, Cognitive impairment induced by Δ^9-tetrahydrocannabinol occurs through heteromers between cannabinoid CB_1 and serotonin 5-HT_{2A} receptors. *PLOS Biol.* **13**, e1002194 (2015).

23. R. G. Pertwee, A. C. Howlett, M. E. Abood, S. P. H. Alexander, V. Di Marzo, M. R. Elphick, P. J. Greasley, H. S. Hansen, G. Kunos, K. Mackie, R. Mechoulam, R. A. Ross, International union of basic and clinical pharmacology. LXXIX. Cannabinoid receptors and their ligands: Beyond CB_1 and CB_2. *Pharmacol. Rev.* **62**, 588–631 (2010).

24. L. W. Crombie, W. M. L. Crombie, D. F. Firth, Synthesis of bibenzyl cannabinoids, hybrids of two biogenetic series found in *Cannabis sativa*. *J. Chem. Soc. Perkin Trans.* **1**, 1263–1270 (1988).

25. T. Takemiya, K. Matsumura, K. Yamagata, Roles of prostaglandin synthesis in excitotoxic brain diseases. *Neurochem. Int.* **51**, 112–120 (2007).

26. L. Mestre, F. Correa, F. Docagne, D. Clemente, C. Guaza, The synthetic cannabinoid WIN 55,212-2 increases COX-2 expression and PGE_2 release in murine brain-derived endothelial cells following Theiler's virus infection. *Biochem. Pharmacol.* **72**, 869–880 (2006).

27. M. D. Mitchell, T. A. Sato, A. Wang, J. A. Keelan, A. P. Ponnampalam, M. Glass, Cannabinoids stimulate prostaglandin production by human gestational tissues through a tissue- and CB1-receptor-specific mechanism. *Am. J. Physiol. Endocrinol. Metab.* **294**, E352–E356 (2008).

28. A. Viader, J. L. Blankman, P. Zhong, X. Liu, J. E. Schlosburg, C. M. Joslyn, Q.-S. Liu, A. J. Tomarchio, A. H. Lichtman, D. E. Selley, L. J. Sim-Selley, B. F. Cravatt, Metabolic interplay between astrocytes and neurons regulates endocannabinoid action. *Cell Rep.* **12**, 798–808 (2015).

29. A. Bilkei-Gorzo, O. Albayram, A. Draffehn, K. Michel, A. Piyanova, H. Oppenheimer, M. Dvir-Ginzberg, I. Rácz, T. Ulas, S. Imbeault, I. Bab, J. L. Schultze, A. Zimmer, A chronic low dose of Δ^9-tetrahydrocannabinol (THC) restores cognitive function in old mice. *Nat. Med.* **23**, 782–787 (2017).

30. M. Waldman, E. Hochhauser, M. Fishbein, D. Aravot, A. Shainberg, Y. Sarne, An ultra-low dose of tetrahydrocannabinol provides cardioprotection. *Biochem. Pharmacol.* **85**, 1626–1633 (2013).

31. C. D. Loftin, H. F. Tiano, R. Langenbach, Phenotypes of the COX-deficient mice indicate physiological and pathophysiological roles for COX-1 and COX-2. *Prostaglandins Other Lipid Mediat.* **68–69**, 177–185 (2002).

32. A. Whelton, Nephrotoxicity of nonsteroidal anti-inflammatory drugs: Physiologic foundations and clinical implications. *Am. J. Med.* **106**, 13S–24S (1999).

33. C. M. Venturini, P. Isakson, P. Needleman, Non-steroidal anti-inflammatory drug-induced renal failure: A brief review of the role of cyclo-oxygenase isoforms. *Curr. Opin. Nephrol. Hypertens.* **7**, 79–82 (1998).

34. D. P. Papahatjis, V. R. Nahmias, T. Andreou, P. Fan, A. Makriyannis, Structural modifications of the cannabinoid side chain towards C3-aryl and 1′,1′-cycloalkyl-1′-cyano cannabinoids. *Bioorg. Med. Chem. Lett.* **16**, 1616–1620 (2006).

35. M. Krishnamurthy, A. M. Ferreira, B. M. Moore II, Synthesis and testing of novel phenyl substituted side-chain analogues of classical cannabinoids. *Bioorg. Med. Chem. Lett.* **13**, 3487–3490 (2003).

36. M. A. ElSohly, Z. Mehmedic, S. Foster, C. Gon, S. Chandra, J. C. Church, Changes in cannabis potency over the last 2 decades (1995–2014): Analysis of current data in the United States. *Biol. Psychiatry* **79**, 613–619 (2016).

37. A. Busquets-Garcia, J. Bains, G. Marsicano, CB_1 receptor signaling in the brain: Extracting specificity from ubiquity. *Neuropsychopharmacology* **43**, 4–20 (2018).

38. C. Defieber, M. A. Ariger, P. Moriel, E. M. Carreira, Iridium-catalyzed synthesis of primary allylic amines from allylic alcohols: Sulfamic acid as ammonia equivalent. *Angew. Chem. Int. Ed.* **46**, 3139–3143 (2007).

39. K. A. Parker, T. Iqbal, New approaches to the synthesis of vitamin D metabolites. 2. Effect of some substituents on stereochemistry in the intramolecular cycloadditions of nonatrienes. *J. Org. Chem.* **52**, 4369–4377 (1987).

40. A. Chicca, S. Nicolussi, R. Bartholomäus, M. Blunder, A. A. Rey, V. Petrucci, I. del Carmen Reynoso-Moreno, J. M. Viveros-Paredes, M. Dalghi Gens, B. Lutz, H. B. Schiöth, M. Soeberdt, C. Abels, R.-P. Charles, K.-H. Altmann, J. Gertsch, Chemical probes to potently and selectively inhibit endocannabinoid cellular reuptake. *Proc. Natl. Acad. Sci. U.S.A.* **114**, E5006–E5015 (2017).

Science Advances

Uncovering the psychoactivity of a cannabinoid from liverworts associated with a legal high

A. Chicca, M. A. Schafroth, I. Reynoso-Moreno, R. Erni, V. Petrucci, E. M. Carreira and J. Gertsch